Power and Spectral Evolution of a Free Electron Laser Oscillator with Electron Beam Energy Ramping

H. S. Marks[a]*, D. Borodin[b], Yu. Lurie[b]
a) Lancaster University, Dept. of Engineering, England, (e-mail: h.marks@lancaster.ac.uk). b) Ariel University, Dept. of Engineering, Ariel 40700, Israel.
Paper submitted 28/12/2020.

***Abstract*— This work is focused on experiments showing enhancements in power extraction efficiency and spectral control of a W-band Free Electron Laser oscillator (FELo) using ramping of the electron beam energy. The FELo operates at 1.4 MeV with electron beam currents of 1-2 A with pulse duration 10-20 μs. Changing the beam energy post-laser-saturation of the initially unbunched continuous electron beam changes the phase-space oscillation trajectory between the beam energy and trapping ponderomotive wave. This enables very significant increases in output power with just 2% changes in beam energy, cases of 39%, and 100% are presented. Unlike in previous work a variable delay has been introduced between the start of the electron beam and the ramp in electron beam energy such that the effect can be observed unambiguously despite significant system jitter from shot-to-shot. In addition to increasing radiative efficiency, where desirable this could be used to rapidly modulate the power without a need to modify parameters such as the beam current or resonator out-coupling. This effect is shown to pull the locked longitudinal modes up or down depending on the direction of the ramp allowing fine frequency control and influence over mode-competition and mode-hops. To complement the experiments simulations were run to map the full range of beam-energy-ramping against resonator out-coupling and beam current for the experimental system.**

***Index Terms*—FEL Oscillator, Regenerative Amplifier, Electron Beam Energy Ramping, Lasing Optimization.**

I. Introduction

Free electron lasers (FEL) operate by extracting radiation from relativistic electron beams [1-2]. The kinetic energy of the electron beams is reduced after oscillatory motion induced by a periodic magnetic or electric field which causes radiation (usually a static magnetic field called an undulator). Some FELs operate in an oscillator configuration, that is, a portion of the radiation generated is contained in the electron interaction region, to increase stimulated emission [3-7]. In the past few years there are ongoing developments related to mm-wave oscillators based on Bragg resonators [8-9], and THz oscillators [10-12].

During lasing there is a resonant interaction between the oscillating electron beam and the stimulated radiation. Changes in the velocity of the electron beam alter the dynamics of that interaction. As the electron beam radiates it loses kinetic energy. To maintain a strong resonant interaction against a falling velocity, changes can be made to the field causing the electrons to oscillate such that as energy is lost, the rate of oscillation is maintained, this is known as undulator tapering [13-20]. Tapering is applied in amplifier and oscillator FEL [21].

Unlike FEL systems in which there is no radiation feedback, oscillators allow the out-coupling of the resonator to be modified to select for an optimal balance between the circulating radiation which drives the lasing and that extracted, this is a well-known principle in lasers [22-23]. Some designs incorporated remote-controlled variable-outcoupling [5, 24]. Pre-bunching the beam is another well-known technique for increasing the extraction efficiency from the electron beam [25-26], applicable to all types of FEL.

It was experimentally demonstrated for the first time that raising the electron beam energy after the laser build-up process (post-saturation) with no undulator tapering can increase the extraction of laser power by around 50%, while maintaining single mode lasing [27]. This occurs as the electron beam is raised to an energetically more favourable synchrotron oscillation path. That work has been recently validated via simulation for the RF-LINAC based FELiCHEM [28]. Their simulation results suggest enhancements in efficiency of 3.6 and 9.1 times at wavelengths of 10 and 30 μm respectively.

In the previous work [27] the electron beam energy ramping was initiated synchronously with the start of the electron beam, this meant that there wasn't a distinct moment in a single pulse at which the change in efficiency could be observed. Jitter in the beam energy from shot to shot made many lasing pulses necessary to demonstrate the increase in radiation power extraction as a result of the ramping. By introducing different delays in timing of the ramping the effect is now demonstrated beyond question over a range of initial beam energy conditions and it is possible to observe its frequency pulling effect (not previously shown). Additionally, in the past work the electron beam energy ramping was presented only for a change in accelerating potential of 20 kV, the simulation was similarly limited. In this paper experimental results are presented in the range 2-30 kV and the simulation provides validation and prediction for a larger range of ramping at all levels of out-coupling and over a range of electron beam currents. Also presented are new experimental results demonstrating the effect of electron beam energy variation post-saturation on the evolution of lasing modes and mode-competition.

The motivation of the study was to demonstrate the lasing-power efficiency enhancement unobscured by system jitter, and to do so over a range of electron-beam energy ramping parameters not previously used while also measuring the effect on the lasing spectrum. The significance is that with a relatively modest investment in equipment for the beamline the electron-beam energy ramping can greatly enhance power output. Within the FEL community the test-setup and mm-wave radiation output of these experiments would be regarded as extremely low energy. However, the results obtained are relevant to THz and IR oscillator systems, and perhaps may be applied to regenerative-amplifier FELs.

The paper is organised as follows: Section I introduces the research objective, motivation, and background. In section II the experimental setup is described. The setup is somewhat unusual as most of the beam-line and interaction region are contained within a high-pressure tank. Section III presents a series of experiments with electron beam energy ramping initiated at different times and levels. Measurement of the frequency dependent roundtrip reflectivity of part of the resonator is shown to explain certain lasing power results. In section IV the effect of the changing electron beam energy on the lasing spectrum is demonstrated. Section V presents simulation of lasing power output over a range of beam energy ramping levels for different levels of transmission from the resonator. These simulations were run for a range of beam currents for an electrostatic accelerator FEL. Finally, sections VI and VII present a discussion of the work and a conclusion.

II. Experimental Setup

A schematic of the electrostatic accelerator FEL based on a Tandem Van-der-Graaf generator on which experiments were conducted and simulations based is shown in Fig. 1. Under normal operation a thermionic cathode provides electron beam pulses of 1-2 A, of 10-20 μs duration. These electron beam pulses are accelerated up to around 1.4 MeV, then enter an equipotential region, the high voltage terminal, where they are focused by quadrupoles for optimal entrance into the resonator (which is encompassed by a planar Halbach undulator). After passing through the resonator the electrons are again focused by quadrupoles before entry into the deceleration tube, at the end of the deceleration tube they are collected. The high voltage terminal is charged with a mechanical belt which introduces significant jitter in the accelerating potential from pulse to pulse, the effect of this on the radiative output power is shown in the next section, although the effect of this jitter is not observed within the time-scale of a single pulse.

During each electron beam pulse a small fraction of the beam continuously strikes the walls of the beam line causing the accelerating potential to fall with time (after a pulse the potential takes several hundred milliseconds to recover before the next pulse can be launched). The change in accelerating potential due to these stray electrons is measured using a Generating Voltmeter (GVM). A GVM generates a current proportional to the potential of the high voltage terminal using two discs in the plane of the tank wall (the plane is normal to the electric field from the high voltage terminal). The outer disc rotates and has segments cut out which alternately let the electric field to pass through or be blocked from the inner complete disc [28].

A voltage-ramping-device (VRD) is connected to the undulator and resonator, its purpose is to compensate for the falling accelerating potential. Under regular operation the resonator and undulator are at the same potential as the sections with the quadrupoles between the acceleration and deceleration tubes. When the VRD is in operation, the resonator and undulator are isolated from the equipotential region between the acceleration and deceleration tubes, isolated also from the parts of the beam line with the quadrupoles [27]. The outer housing of the undulator and resonator which is opposite the GVM is at the same potential as the high voltage terminal. Therefore, the increasing potential on the resonator due to the VRD is not measured with the GVM. As such we can estimate the total change in accelerating potential using the known charging profile of the VRD and the measured voltage fall rate due to stray electrons. The main properties of the EA-FEL are summarised in Table I and described in a previous publication [24].

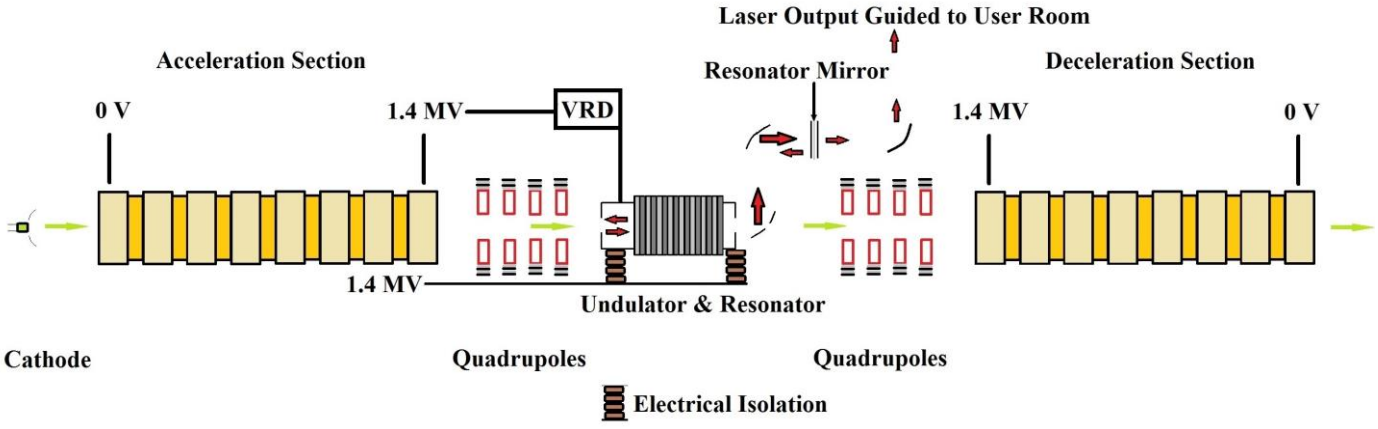

Fig. 1. Schematic of the EA-FEL based on a Tandem Van-der-Graaf generator. The electrons are generated using a thermionic cathode. They are injected into an acceleration section, which is located within a high-pressure tank where they are brought to near the speed of light. Beyond this, they are focused with

quadrupoles into the undulator and resonator combination to generate laser radiation. The electrons enter and leave the resonator through on-axis holes in mirrors at either end of the resonator. Once the electrons leave the resonator, they are re-focused and decelerated. Within the resonator the lasing radiation develops an interference pattern such that it is split either side of the holes at each of the electron-entrance and electron-exit mirrors due to transitions between different waveguide sections. The mirror through which the electrons exit reflects the lasing W-band radiation upwards and via a second mirror to the exit out-coupling mirror. The exit mirror is formed from three wire-grids, the middle of which rotates, the reflectivity of this mirror is controlled from the user room via the rotation angle. The laser radiation reaches the user room via sections of circular corrugated waveguide. Free-space transmission is used to get the radiation from the high-voltage region to the region of the high-pressure tank at ground potential.

TABLE I: Properties of the EA-FEL

Beam Current	1-2 A
Beam Energy	1.35-1.45 MeV
Undulator Period	44.4 mm
Effective No. of Undulator Periods	24
Undulator field Amplitude	1.93 kG
Waveguide Fundamental Mode	HE_{11}
Radiation Frequency	95-110 GHz

The lasing pulses reaching a user station are sampled by reflecting -32 dB of the signal aside, and after further attenuation measuring the power and frequency using a mixer (Quinstar QMB-FB BB W) and a crystal detector (Millitech DXP-10 RPFW0). The local oscillator signal is generated using an HP sweep oscillator 86290B set to continuous wave output and multiplier (Millitech 380 AMC 10-RFH00 A16800). The mixed signal is recorded on a Keysight DSCX3104A 5 GS/s, 1 GHz bandwidth oscilloscope.

III. Experimental Results—Analysis of Power Output

Using the setup described in Section II, a series of experiments are presented which demonstrate the effect on the power output and spectrum of ramping the electron-beam-energy. The foremost matter is to establish beyond doubt that the claimed rise in lasing power is due to ramping of the electron beam energy. In the previous work the ramping was synchronous with the start of the electron beam pulse and the effect emerged from the statistics of many pulses [27]. By initiating a rise in electron-beam energy only after the lasing mode has been established for several microseconds the effect can be decoupled from the normal jitter of operation. This is demonstrated in Fig. 2 which is a plot of the lasing power at the resonator exit as a function of time.

In Fig. 2, time zero is the start of a 1.17 A continuous electron beam, this beam is abruptly stopped at 18.8 μs. The electron beam energy falls with time from 0 μs until 4.6 μs due to stray electrons discharging the built-up accelerating potential. At 4.6 μs the electron-beam energy ramping is initiated with the VRD. This increases the electron energy by ~30 keV with a charging time constant of ~0.8 μs. The falling beam energy causes the lasing power to drop for the locked single frequency (for these pulses ~100.497 GHz). The average voltage fall rate of the high voltage terminal due to stray electrons discharging the high voltage terminal in these shots is 1.48 kV/μs with a standard deviation (SD) of 0.07 kV/μs. In each case of the 11 shots presented in Fig. 2 the ramping initiated at 4.6 μs causes the power to rise to a value which exceeds the initial peak by an average factor of 1.17. There is significant shot-to-shot jitter due to fluctuations in the accelerating potential caused by the charging method (a mechanical belt). The out-coupling of the resonator is set such that power transmission is 23% and total power roundtrip reflectivity is ~50%. At 17 μs the effect of the ramping is undone as the resonator is deliberately discharged, reducing the potential difference from 30 kV to 0 kV, to show the effect on the power. Three effects can be observed in Fig. 2: Firstly the drop in output power due to the normal continuous drop in accelerating potential after the lasing has been established and reached some peak. Second the reversal of this fall in output power, and rise to a point above the initial maximum power, showing an enhancement in efficiency. Thirdly, the rapid decrease in power as the accelerating potential is rapidly reduced at 17 μs.

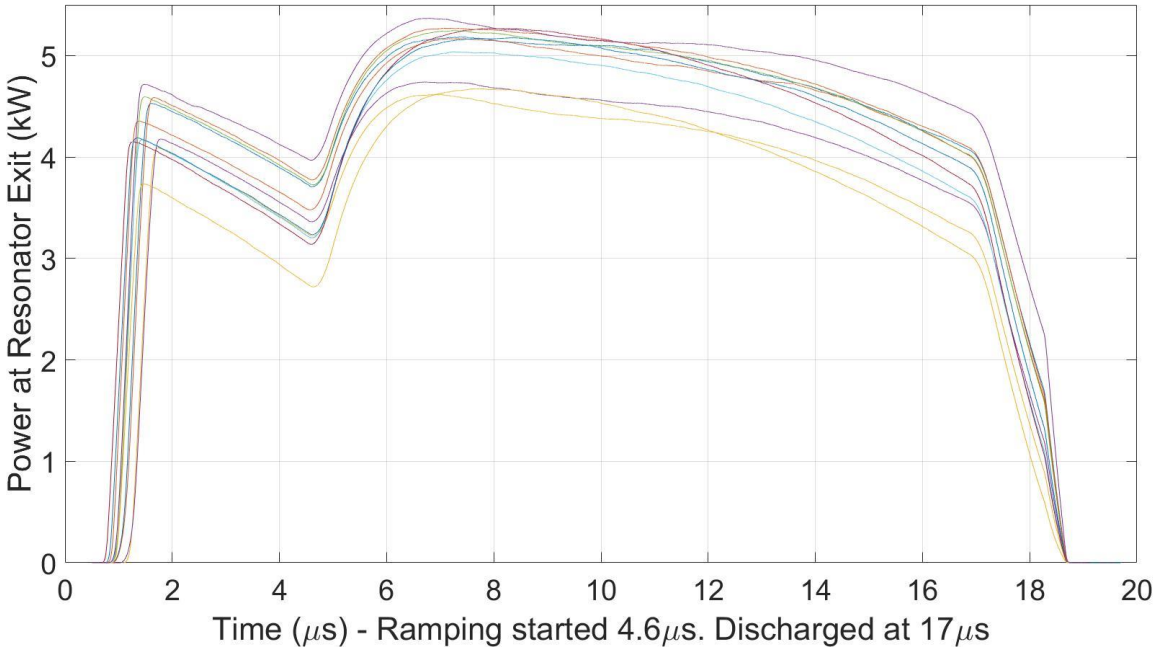

Fig. 2: Power at the resonator exit as a function of time for a 1.17 A continuous electron pulse of 18.8 μs with resonator power out-coupling (transmission) at 23%. At 4.6 μs, 30 kV ramping of the electron beam is initiated, at 17 μs the charged-up resonator is abruptly discharged.

The net increase in accelerating potential in Fig. 2 at 6.5 μs (when the highest peak in power is observed) relative to that at the start of the electron beam is approximately 20 kV. The ramping is set to 30 kV but stray current causes a ~1.48 kV/μs reduction in the accelerating potential of the high voltage terminal. By reducing the delay time in initiating the voltage ramping, the peak net increase in accelerating potential can be greater. In Fig. 3 the conditions are the same as described for Fig. 2, except that now the ramping is started at 1.5 μs, shortly after the radiation power reaches its initial peak. The built-up charge on the resonator is discharged at 13.8 μs, though the electron beam isn't stopped until 18.8 μs. The average fall rate of the high voltage terminal is 1.38 kV/μs with a SD of 0.05 kV/μs. The net increase in electron beam energy, deducting the fall in voltage of the high voltage terminal before peak-power is established at 3.4 μs is 25.3 kV. This contrasts with the maximal net increase of 20 kV in Fig. 2. Due to the ramping occurring earlier in the pulse the average change from the initial to final peak power is a factor of 1.39. This altering of the timing of the ramping between Fig.2 and Fig. 3 is another clear demonstration that it is the ramping of the beam energy which is causing the increase in efficiency.

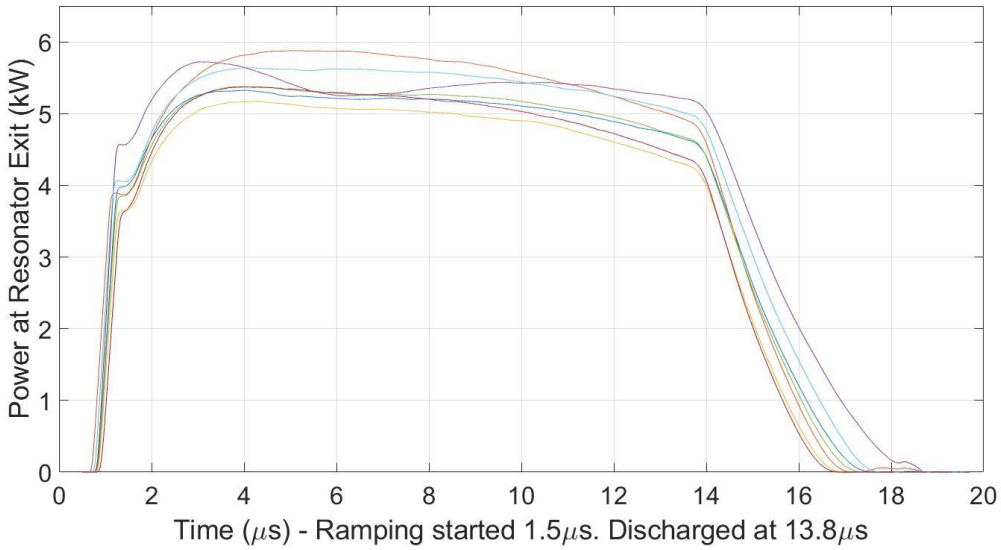

Fig. 3: Power at the resonator exit as a function of time for a 1.17 A continuous electron pulse of 18.8 μs with power transmission at 23%. At 1.5 μs 30 kV ramping of the electron beam is initiated, at 13.8 μs the charged-up resonator is abruptly discharged.

Figures 2 and 3 presented results of power output at the maximum ramping level achievable with the setup, 30 kV. As part of the same series of experiments as the results of Fig. 2 and 3, the ramping voltage was reduced in steps to show the effect at different ramping levels. These results are presented in the seven curves plotted in Fig. 4, ranging from 28 kV down to 0 kV. The average fall rate of the high voltage terminal is 1.52 kV/μs with a SD of 0.12 kV/μs. It is clear raising the ramping level increases the useful radiation extraction efficiency, although it was not possible in this experiment to raise the ramping level to a point which would diminish power in the lasing mode.

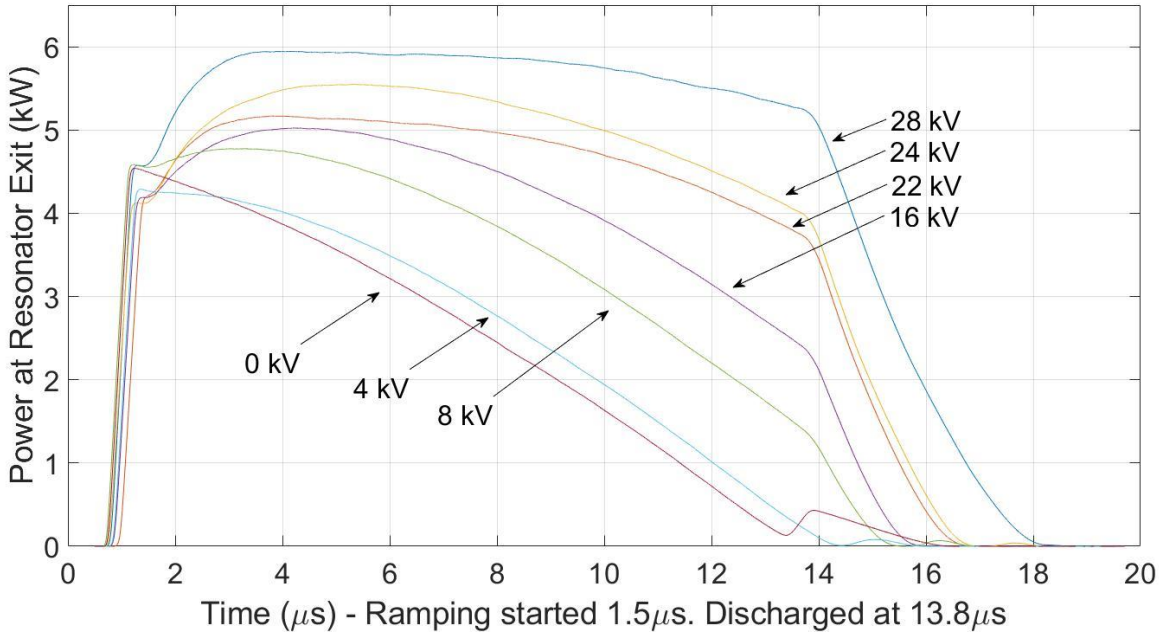

Fig. 4: Power at the resonator exit as a function of time for a 1.17 A continuous electron pulse of 18.8 μs with power transmission at 23%. At 1.5 μs ramping of the electron beam is initiated at levels of 28, 24, 22, 16, 8, 4, and 0 kV; at 13.8 μs the charged-up resonator is abruptly discharged.

Figure 5 is a plot of sixteen 98.7 GHz lasing pulses recorded minutes apart with a 1.07 A beam for which the transmission was 27% and the total roundtrip reflectivity 43%. For six pulses ramping is initiated at 2.03 μs, for five pulses the ramping starts at 5.75 μs, and for five pulses 9.1 μs, the electron beam is stopped at 17.4 μs, for some of the pulses the ramping voltage is discharged at 16.5 μs. The average fall rate of the high voltage terminal is 1.09 kV/μs with a SD of 0.04 kV/μs. In the case of the lowest curve the power is just 140 W when the ramping is initiated, roughly 0.15 μs away from extinction of the lasing mode. The power is brought up to 2.37 kW, demonstrating a remarkable ability to dynamically and rapidly alter the power within the pulse up and down. Note the initial peak power of these pulses is roughly half that of those in figures 2-4. This can be explained in part by the higher internal losses of the resonator at this frequency combined with the higher out-coupling and lower electron beam current. One way the higher internal resonator losses can be discerned from the graph in Fig. 5 is the longer average build-up time before the sharp rise in power begins, in Fig. 4 this is ~0.74 μs, whereas in Fig. 5 it is ~1.23 μs. The average powers for the three cases of ramping initiated at 2 μs, 5.75 μs, and 9 μs, are 3.5 kW, 3.9 kW, and 3.1 kW respectively. At first it may seem like there is a contradiction; in figures 2 and 3 initiating the ramping earlier increases the output power, but in Fig. 5 of the three ramping times the highest average power is for not 2 μs but 5.75 μs. The apparent contradiction may be resolved by noting that the lasing pulses of figures 2-4 are produced at ~100.497 GHz, whereas the lasing pulses of Fig. 5 were at ~98.7 GHz. The roundtrip losses are higher at the lower frequency as is explained below and shown in Fig. 6. The higher losses result in a smaller oscillating electric field within the resonator, that is a less large potential trap for synchrotron oscillations. With a smaller potential-trap it is easier for electrons to become de-trapped by a rising beam energy and so radiate significantly less. This is shown in the simulation results of figures 12 and 13 in which raising the beam energy beyond a certain level reduces output power. The negative effect on the beam power occurs at a lower ramping level in Fig. 12 than in Fig. 13 as the fixed roundtrip losses are higher. In summary, for the curves in which ramping is initiated at 2 μs the electrons are moved past the optimum point for energy extraction. From 2 μs to 5.75 μs the beam energy drops on average 4.1 kV. Applying the ramping at 5.75 μs brings the electron energy to a point in the potential trap more favourable than that at 2 or 9 μs.

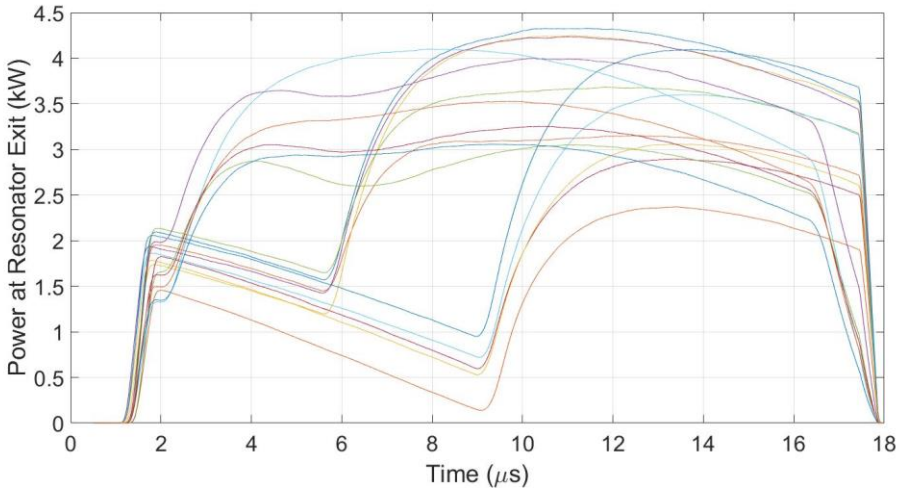

Fig. 5: Power at the resonator exit as a function of time for sixteen 1.07 A continuous electron pulses. Voltage ramping of 30 kV is applied, for six pulses it is initiated at 2.03 μs, for five pulses 5.75 μs, and for five pulses 9.1 μs. The electron beam is stopped at 17.4 μs, for some of the pulses the ramping voltage is discharged at 16.5 μs, Note the rise time for these curves is slower than those of figures 2 & 3, an average of 1.23 μs instead of 0.74 μs. The lasing frequency is ~98.7 GHz and resonator transmission 27%.

To understand the spectrum of lasing modes it is important to understand the frequency dependent roundtrip reflectivity (Rrt) of the resonator cavity. The electron beam enters and leaves the resonator cavity through holes in the centres of the mirrors at either end of the resonator cavity. To avoid a large part of the lasing power being lost to these on-axis holes, Rivlin-Denisov splitting (analogous to the Talbot effect) was used [30-32]. In the main interaction region of the resonator the waveguide is corrugated, and the radiation built up is in the transverse HE_{11} mode. The maximum intensity of this mode is at the centre of the waveguide. To avoid a significant part of this being lost through the holes in the entrance and exit mirrors, a transition is made to a wider smooth walled waveguide which excites new transverse waveguide modes. The interference pattern generated after the transition is such that the lasing power is split either side of the hole in the mirror. The advantage of this is that power is not lost to the hole in the mirror. However, the distance at which the split interference pattern forms is frequency dependent. For this reason, the Rrt has a strong frequency dependence. At the entrance section of the resonator the lasing radiation pattern is split and reflected-back along the axis on which the electrons travel. At the exit of the resonator the split lasing radiation pattern is reflected off-axis in order to de-couple it from the electron beam. It is the more-complex waveguiding structure at the exit which causes most of the internal losses. A wideband measurement of the Rrt of this end-section of the resonator connected to a corrugated waveguide is plotted in Fig. 6. Note, S11 is a measure of the ratio of the reflected wave divided by the transmitted or initial field at the input port.

The Rrt is at maximum close to 102 GHz, it decreases above and below this frequency. The frequency dependence of the Rrt influences the mode competition. As such it is possible that the mode that wins the mode-competition does not coincide with the maximum of the small signal gain. The electron beam energy for the results presented in Fig. 5 is below that for the results in figures 2-4, and so the lasing frequency is lower. It is possible that the dominant mode established for the pulses in Fig. 5 is at a frequency just above the maximum of the small signal gain due to the strong frequency dependence of the Rrt effecting the mode competition. That is, the optimal initial gain (detuning from synchronism) was for a frequency several hundred MHz below 98.7 GHz but the higher feedback at 98.7 GHz caused power to grow at a faster rate for this mode. The increase of Rrt from 96 GHz to 102 GHz influences the mode competition. This may explain why the relative change in lasing power is much greater in Fig. 5 when compared with figures 2 and 3. In Fig. 5 the lasing starts initially at a sub-optimal gain point due to the strong frequency dependence of the resonator. For this reason, an increase in electron-beam-energy has a greater effect than when for instance the maximum of the Rrt coincides with the maximum of the gain.

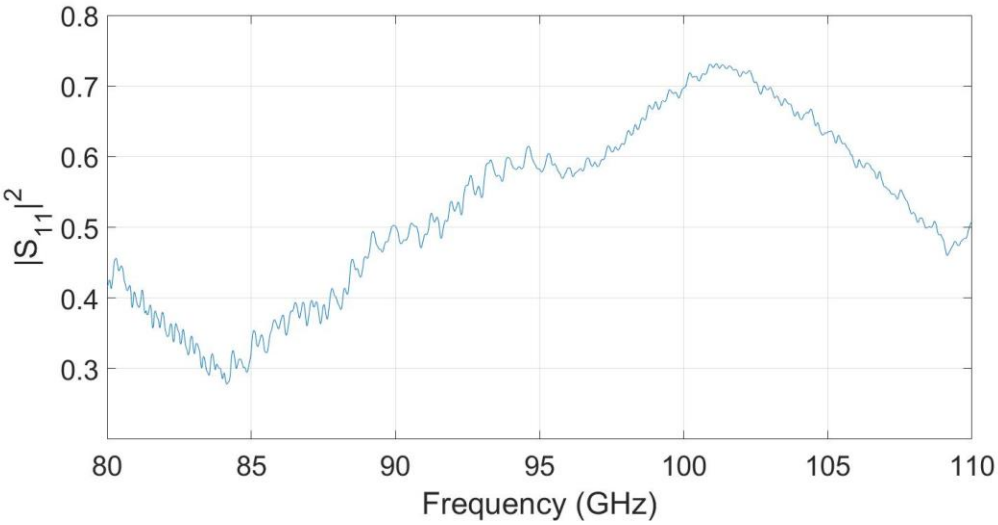

Fig. 6: Roundtrip reflectivity measurement of $|S11|^2$ of the main frequency dependent element of the resonator which decouples the electron beam from the radiation via Denisov splitting, a modern mm-wave version of the Talbot effect.

To summarize what has been demonstrated in figures 2-5, lasing is established at a frequency close to that for which the beam-energy detuning from the FEL synchronism condition is initially optimal during the build-up process. However, once power has built up the initial beam-energy detuning from the FEL synchronism condition is no longer optimal as the conditions have changed significantly with vastly increased power circulating in the resonator. Increasing the beam energy allows for a greater exchange of energy from the electron beam to the massively increased circulating radiation. When the beam energy is dropping this is also a demonstration of the same effect but moving to a less efficient electron beam energy for radiation extraction.

IV. Experimental Results—Analysis of Lasing Spectrum

In the lasing pulses shown in figures 2-5, typically, after a 1-2 μs period of mode competition a dominant mode emerges which is locked, and keeps lasing despite changes in accelerating potential until the gain drops sufficiently and a new mode emerges hundreds of MHz away from the previous one. There are two effects on the lasing spectrum due to the electron beam energy ramping which go together with the changes in lasing power: 1) The frequency of a locked mode is pulled up or down according to the ramping direction. 2) Non-dominant modes are also locked and pulled, this will cause new-modes to arise after a mode-hop deviated from the frequency they would be locked to at the start of the process.

The spectrum is measured using a mixer which has as its input the attenuated lasing signal (the RF) and a known stable reference frequency, known as the Local Oscillator (LO). The mixer provides an output known as the Intermediate Frequency (IF), the IF is the absolute value of the difference between the RF and LO such that no distinction is made in the output between when RF > LO or RF < LO. Assuming a single lasing mode, if the LO is set above the RF (lasing frequency) then if the lasing frequency drops with time due to a falling accelerating potential then the IF would increase with time. Conversely, if the lasing frequency is rising with the LO set above the lasing frequency the IF will fall with time.

The first frequency pulling effect is demonstrated in Fig. 7, which shows Fast Fourier Transforms (FFTs) of four of the five pulses shown in Fig. 5 for which the ramping is delayed to 9 μs. The three curves in each graph represent FFTs from 1.8-3.8 μs, 7-9 μs, and 12-14 μs. The centre curve (blue dashed line) is for the period 1.8-3.8 μs, the rightmost (red) is for 7-9 μs, from 1.8 to 9 μs the IF frequency increases, even though the power is dropping, this is because the Local Oscillator is set above the lasing frequency. From the middle of the first period, 2.8 μs to the middle of the second at 8 μs the average drop in lasing frequency is ~2 MHz, from 8 μs to 13 μs the overall increase in frequency is ~3.8 MHz. This frequency pulling effect of an increase or decrease in lasing frequency when the electron-beam-energy is increasing or decreasing is observed in every set of data.

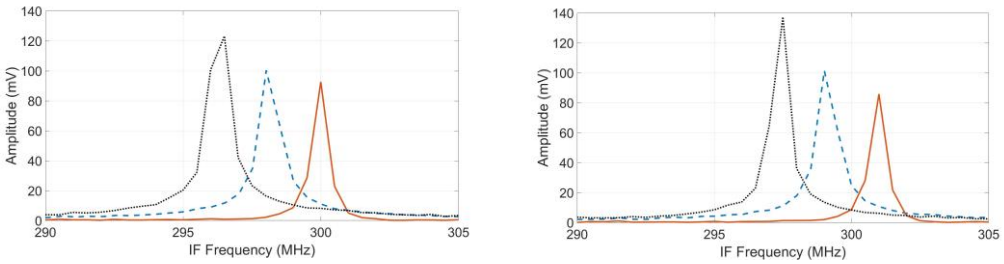

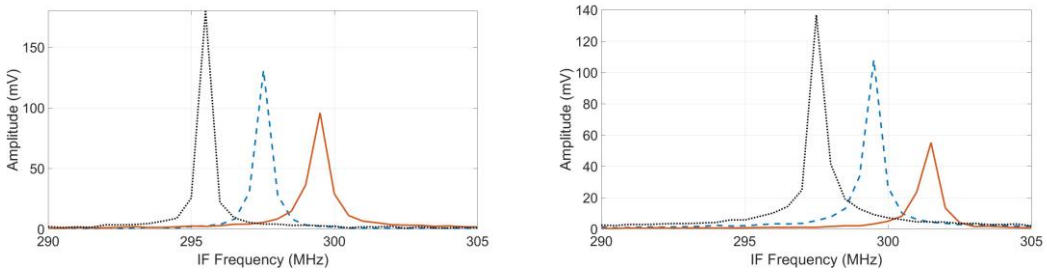

Fig. 7: Four graphs of FFTs performed in Matlab of four of the five pulses shown in Fig. 5 for which the ramping is delayed to 9 µs. The three curves in each graph represent FFTs from 1.8-3.8 µs, 7-9 µs, and 12-14 µs. The centre curve (blue dashed line) is for the period 1.8-3.8 µs, the rightmost (red) is for 7-9 µs, from 1.8 to 9 µs the IF frequency increases, even though the power is dropping, this is because the Local Oscillator is set above the lasing frequency.

The second observation regarding non-dominant modes being pulled is demonstrated in figures 8-10. In Fig 8. a lasing power-profile is plotted as a function of time. The initial and final power after ramping are lower than previous pulses shown, its instability allows the mode-competition to be observed over a longer period. As a visual aid to get an overview of the mode-competition process occurring in Fig. 8 a spectrogram is plotted in Fig. 9. The spectrogram shows the IF as a function of time, the spectrogram in Fig. 9 is calculated using 0.5 µs windows with an overlap of 4 ns, and a sampling frequency of 5 GHz. Voltage ramping to 30 kV is begun at ~2 µs. The dominant mode which prevails having an IF of ~911 MHz is above the 102 GHz LO frequency. Initially the mode with the most power, before ramping, is at 815 MHz. At around 1.5 µs modes below the LO have enough power to be measured, but the voltage ramp pulls the power back to the higher frequency modes.

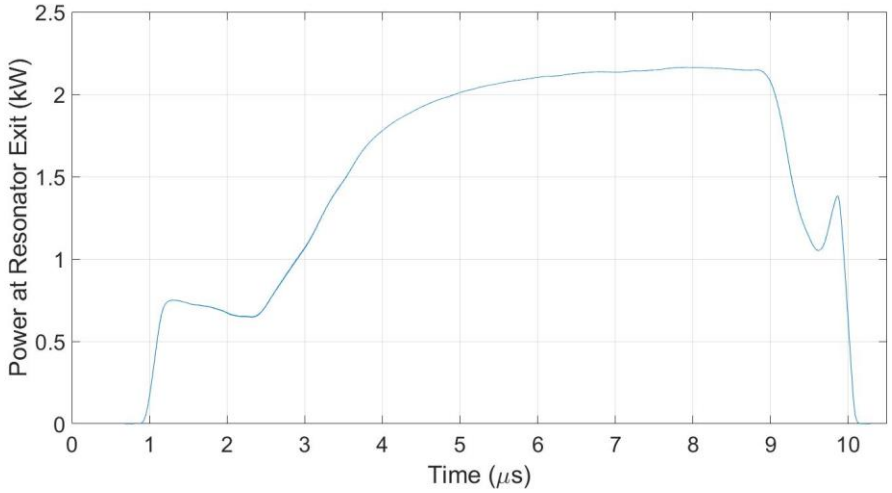

Fig. 8: Power profile of a lasing pulse at the resonator exit. Voltage ramping of 30 kV is started at ~2 µs. Resonator power transmission 18.6%.

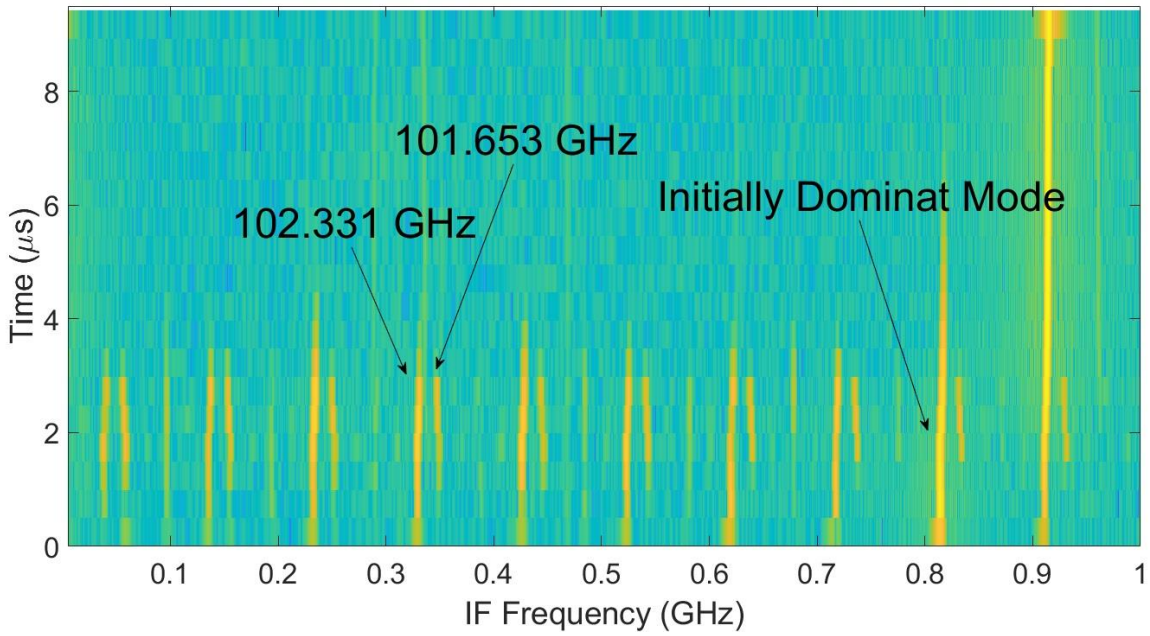

Fig. 9: Spectrogram plot providing a qualitative overview of the mode competition. The LO is set to 102 GHz, the mode that prevails is at a frequency of 102.911 GHz. Resonator power transmission 18.6%.

In Fig. 10 two FFTs of the IF data seen in Fig. 9 are presented over the range 210-460 MHz for time windows 1.08-2.64 μs (blue curve), and 2.64-4.20 μs (red dashed curve), a limited frequency range is chosen just for readability. The frequency modulation of the modes reduces the FFT amplitudes. The LO is set to 102 GHz, in the IF data we see modes above and below the LO, as IF = |RF-LO|. One of the ways the modes above and below the LO can be distinguished is by the direction of frequency chirp when the electron beam energy increases or decreases. Though we see many longitudinal modes, only a single transverse mode, HE_{11}, is excited in the main interaction corrugated waveguide region. Therefore, we know the real frequency separation between adjacent lasing modes is ~97 MHz. In Fig. 10 there are two arrows pointing to the centre peaks in the graph. These centre modes appear adjacent, separated by ~20 MHz, however, they are on different sides of the 102 GHz LO, their separation is ~678 MHz. Such that one arrow points to 102.331 GHz, the other to 101.653 GHz. When the lasing modes are pulled to higher frequency due to ramping up of the electron beam energy, those modes above the LO move to a higher IF, while those below the LO shift to a lower IF. From the first time-period (blue curve) to the second time-period (red dashed curve) the frequencies of the labelled centre peaks appear closer-together on the plot. In fact, the frequencies of all modes are increasing in frequency due to the ramping, maintaining the separation of longitudinal modes.

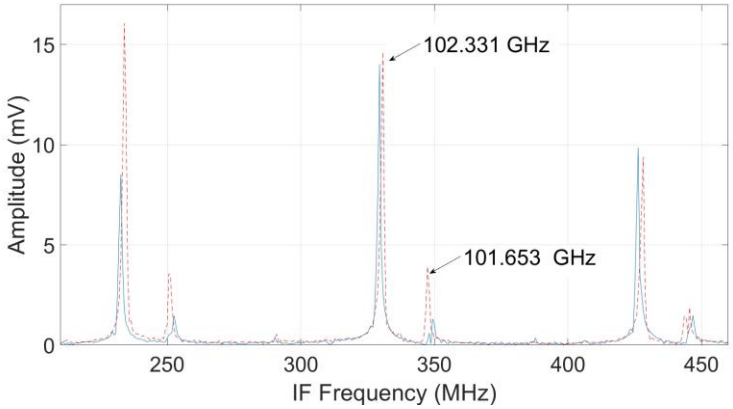

Fig. 10: Plots of two FFTs taken at different time intervals of the pulse shown in figures 8 and 9 showing the IF frequency range 210-460 MHz, first FFT time window (blue curve) 1.08-2.64 μs. Second FFT time window (red dashed curve) 2.64-4.20 μs.

Figure 11 is an FFT over the same time periods as Fig. 10 but shows the modes over an 800-935 MHz range. In the first time-window (blue curves), of the two adjacent competing modes at 102.814 and 102.911 GHz, the lower frequency is dominant. In the second period after ramping is initiated both modes are pulled to higher frequencies, and the power shifts to the higher frequency mode which becomes the dominant lasing mode.

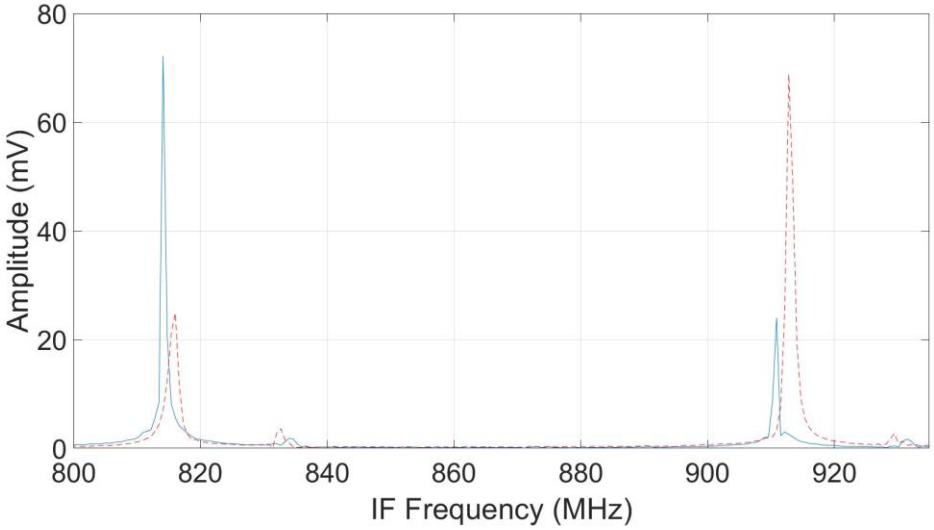

Fig. 11: Plots of two FFTs taken at different time intervals of the pulse shown in figures 8 and 9 showing the IF frequency range 800-935 MHz, first FFT time window (blue curve) 1.08-2.64 μs. Second FFT time window (red dashed curve) 2.64-4.20 μs.

V. Simulating Maximal Extraction By Beam Energy Ramping

To simulate the effect of beam energy ramping over a much wider range of parameters than was practical with experiment the electron-radiation interaction dynamics code FEL3D was used [33]. The simulation code is a steady state, single frequency, and single pass (amplifier) program, three-dimensional effects due to a finite beam size and a non-uniform profile of the undulator magnetic field are incorporated. Previously simulations were run for 20 kV beam energy ramping at one current and a fixed level of resonator outcoupling. Below, the parameter space for this system in relation to electron beam energy ramping is mapped as a function of out-coupling for a range of ramping levels and for different electron beam currents.

Each of the simulations began with a constant beam energy of 1.4035 MeV, 1 μs after lasing saturation is reached the beam energy is changed to a given ramping level. The constant value of the beam energy before ramping and then after the ramping stand in contrast to the experiments in which the beam energy was falling at in the case of Fig. 2, 1.48 kV/μs. The power level post-ramping at the new saturation level is used to calculate the power out of the resonator.

Results of FEL3D simulations of extracted power for a given beam energy ramp with a fixed 1.13 A current (close to that used in many previous experiments) and fixed roundtrip losses of 35% (and the parameters in Table I) are depicted in Fig. 12. There are seven curves plotted, each showing the peak power out from the resonator as a function of the transmission from the resonator when different increments in accelerating voltage are applied post laser-saturation. The bottom curve corresponds to no voltage ramping (0 kV), that is a constant beam energy of 1.4035 MeV, this is the initial energy for all the data points before the voltage ramp. It corresponds to the maximum of the small signal gain at the frequency oscillating in the resonator (101.85 GHz). The curve above this, a 5 keV increment in beam energy post laser-saturation, and so forth.

The range of transmission from the resonator at which the laser will operate is reduced by the rise in beam energy, the roundtrip reflectivity becomes insufficient. Without ramping lasing is predicted to cease for a transmission of around 0.55, whereas for 15 kV ramping the point is around 0.4. This cessation in lasing following the increase in beam energy is a result of the electrons becoming de-trapped from the potential generated by the stored oscillating radiation. This is clear by contrasting the level of transmission at which lasing ceases for different voltage ramping levels in figures 12 and 13, Fig. 12 is different from 13 only in that the fixed resonator loss has been reduced to 15% from 35%.

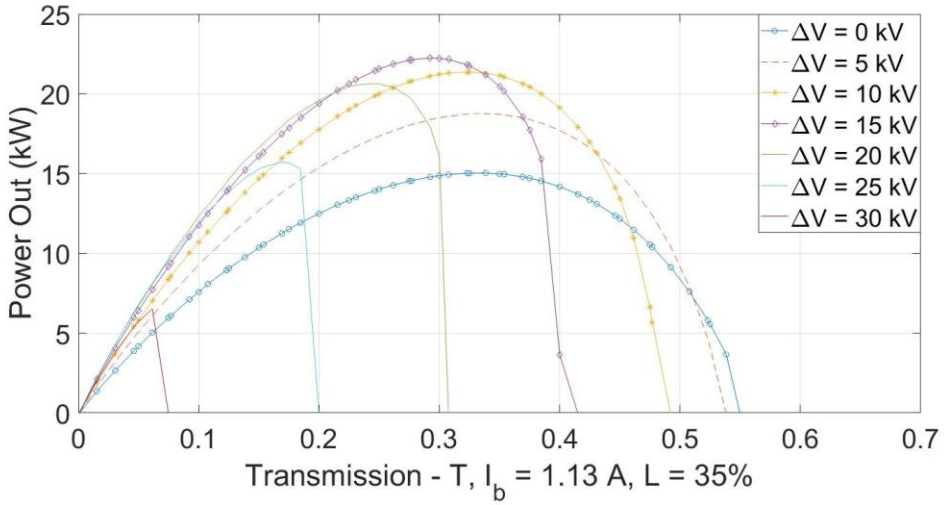

Fig. 12. Power transmitted (kW) from the resonator as a function of the transmission from the resonator for seven levels of changes of electron beam energy post laser-saturation. The beam current was fixed at 1.13 A, whilst the fixed roundtrip losses were set to 35%. Electron beam energy 1.4035 MeV.

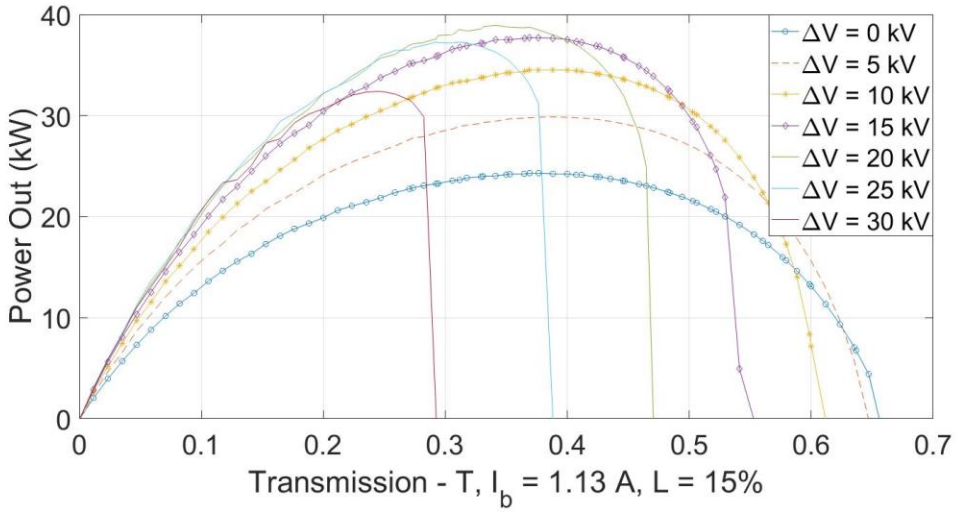

Fig. 13. The Power transmitted (kW) from the resonator as a function of the transmission from the resonator for seven levels of changes of electron beam energy post laser saturation. The same 1.13 A beam current and 1.4035 MeV beam energy as Fig. 12, but with fixed roundtrip loss of 15% almost twice the peak power is reached.

Now we consider electron-beam-ramping as a function of the electron beam current. First considering in Fig. 14 simulations for the power from the resonator for five currents, 1.13 A, 3 A, 5 A, 7 A, and 9 A; as a function of the transmission from the resonator for fixed roundtrip loss of 35%. Compared to the relatively symmetric output from the resonator for the no-ramping case of figures 12 and 13, these curves are skewed with the peak power near the maximum transmission before lasing is extinguished. It is a transition towards a different FEL operating regime, that of the regenerative amplifier where only a small fraction of the power generated needs to be re-circulated. With less feedback required the resonator designed for high power output (>7 A) can be simplified from the existing design [32], reducing losses as so little feedback is required.

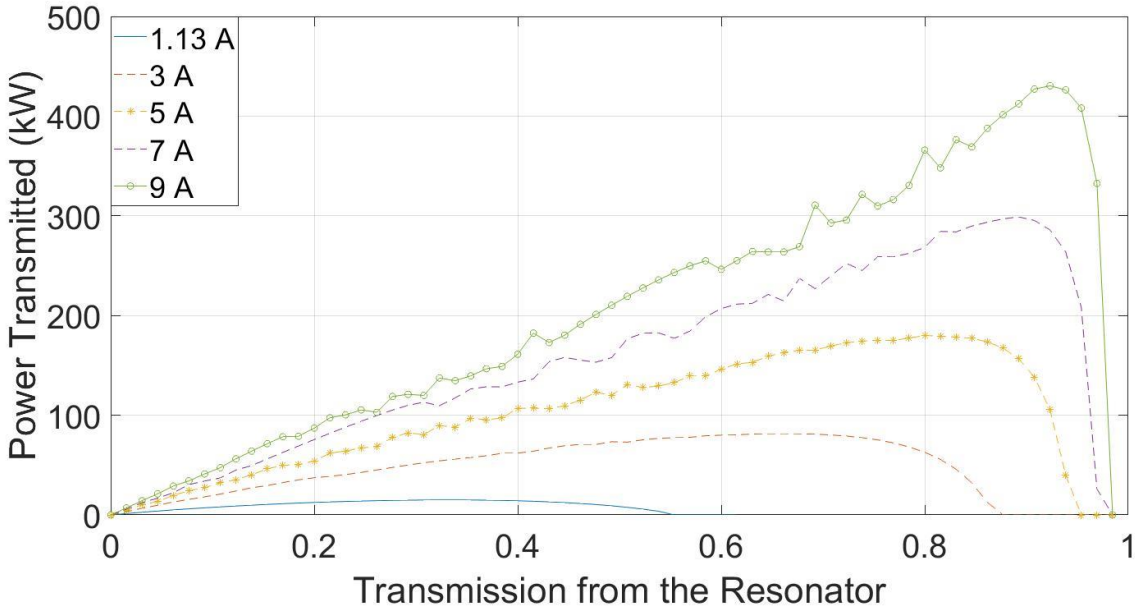

Fig. 14. For fixed roundtrip loss of 35% and FEL parameters given in table I, the power out from the resonator is plotted as a function of the transmission from the resonator for five different electron beam currents.

We can consider for an EA-FEL the efficiency as a function of the beam current (without any change in beam energy). This is shown in Fig. 15 in which the power out from the resonator, normalized by the beam current, is plotted against the transmission from the resonator. The general trend is a linear increase in power extraction efficiency of the EA-FEL oscillator for higher transmission, until a turning point is reached. At higher currents the turning point is at higher transmission, allowing for greater efficiency. The reason in part for the approximately linear dependence is because the circulating power ΔP for the currents greater than 3 A is approximately constant over a wide range of roundtrip reflectivity. The power out from the resonator is proportional to the transmission. If the internal losses were lower, for instance 15% the curves would not appear linear [34].

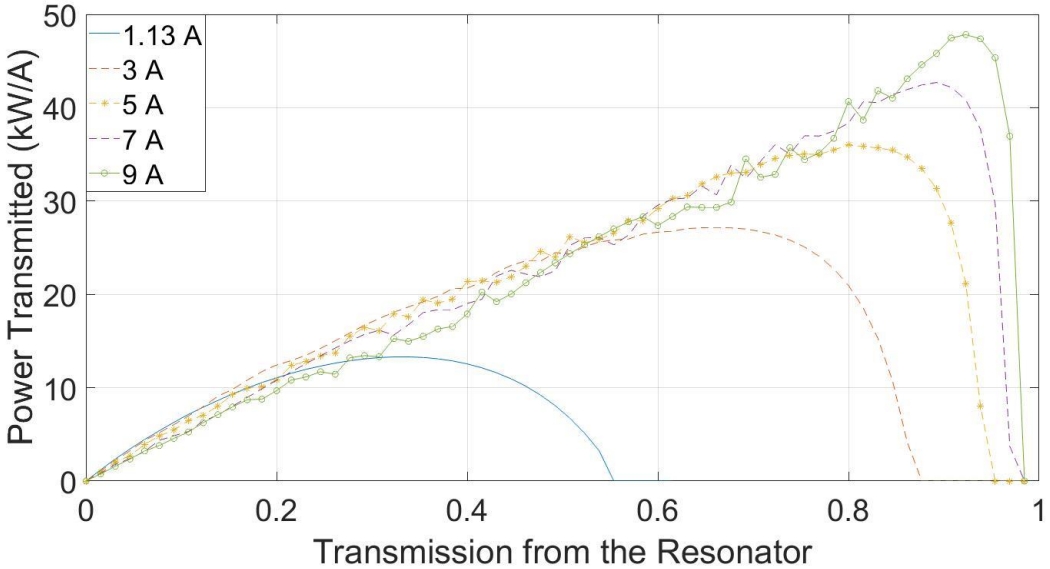

Fig. 15. For fixed roundtrip loss of 35% and FEL parameters given in table I, the power from the resonator normalized by the beam current is plotted against transmission from the resonator.

In Fig. 15, the maximum radiation power per unit beam current is at 9 A, so with this current the voltage ramping is explored. With a cathode capable of emitting 9 A (not currently implemented), 425 kW output power can be brought up to 850 kW with a lasing time limited only by the supply current and beam loss (which reduces the accelerating potential). This could be a powerful source of extremely narrow linewidth radiation for which the frequency could be chirped in a controlled manner during the pulse. The bottom (blue) curve in Fig. 16 is with no voltage ramping. The curve above this is for a 10 keV increase in beam energy, 20

keV for the curve above that, and so forth, raising the beam energy beyond 55 keV to 60 keV (or above) is detrimental to power extraction.

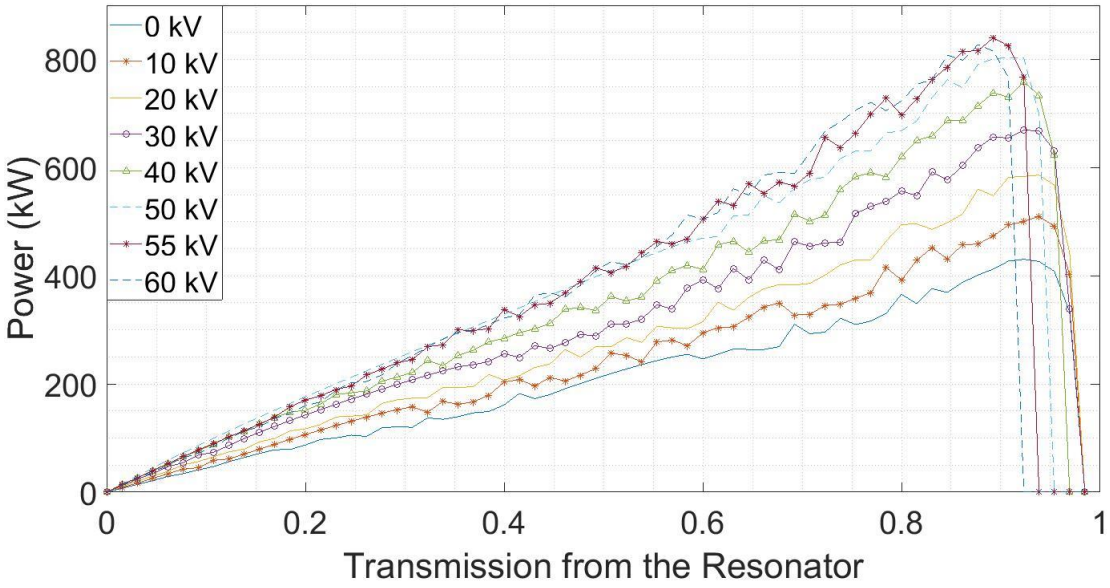

Fig. 16. Examining the impact on a 9 A beam current of voltage-ramping. The bottom curve is without voltage ramping. For each curve above the beam-energy has been increased 10 kV, until the final two transitions from 50 to 55 kV, where the maximum is reached, and 60 kV where the fall in extraction begins. Roundtrip losses are fixed at 35%.

There is precedent using a high current thermionic cathode with an electrostatic accelerator, the Dutch FOM FEM used a 12 A thermionic cathode [5], voltage ramping would have been quite simple to implement in their inverse setup in which the resonator and undulator sit outside the high-pressure tank. Unfortunately, this system has long since been dismantled.

VI. Discussion

The simulations run at 1.13 A predict higher output power than recorded during the experiment for similar out-coupling, however, in recording peak powers from the simulation there was not falling beam energy or mode competition. As well, for the simulation the electron beam was mono-energetic with an ideal trajectory and the simulated resonator was not dispersive always assuming lasing at the lowest internal loss point of the resonator (35%). By contrast in the experimental results of Fig. 5 the internal loss is estimated to be 43%.

The roundtrip losses which have been specified in the paper are based on measurements of the resonator without the gain medium, the electron beam. A likely source of loss in this system not previously considered may arise due to a section of the Talbot-splitting part of the resonator being within the undulator. Gain in this region would change the distribution of the transverse modes causing increased loss at the mirror through which the electrons leave the resonator. Also reducing the coupling of the back reflected wave into the main interaction region (a corrugated waveguide). The corrugated waveguide is encompassed by 20 periods of the undulator. The Talbot sections at either end of the resonator are encompassed by a further three undulator periods each (in total there are 26 undulator periods). It was previously estimated that the effective number of undulator periods was ~24 due to the overlap of the electric field on-axis with the electron beam. Assuming the growth of power in these sections causes increased overall loss then the simulations would better reflect the experiment with closer to 20 periods. The Talbot-splitting parts of the resonator which are partially encompassed by the undulator are placed in this way due to the very difficult mechanical constraints of the system. The constraints are a result of the system being originally designed as an ion-accelerator but being converted into an FEL once it was no longer in use for ion-acceleration. It may be beneficial to re-design the resonator.

The experimental system has been continuously and reliably running for around eight years since its last maintenance and inspection cycle. It's also possible the resonator feedback may be more degraded than estimated due to stray electrons hitting the exit mirrors of the resonator. The lasing pulses recorded in the experiments could have been continued to around 50 μs but the electron beam was typically stopped at less than 20 μs, this was to ensure that the IF data would be recorded by the oscilloscope at the maximum sample rate.

VII. Conclusion

In the previous work [27] which was the first theoretical and experimental demonstration of the efficiency enhancement derived from electron beam energy ramping, the ramping was synchronous with the start of the electron beam; many pulses were required to demonstrate the effect due to inherent system jitter. In this work the effect is unambiguously demonstrated using a variable delay in the time before beam energy variation. The variation in beam energy allows rapid modulation of the output power without recourse to changing the beam-current or resonator out-coupling. It is shown that competing modes are locked and pulled up or down in frequency with the beam energy variation. Allowing if desired an option for a fine frequency sweep during a single pulse. The simulations have shown the range of the effect for different steps in beam energy with variable transmission, and that the efficiency of the enhancement grows with increasing beam current where less feedback is required. Suggesting this effect might be usefully employed in a regenerative amplifier. The electron beam energy ramping can be used in addition to other power optimisation techniques such as optimising for radiative out-coupling and pre-bunching.

References

[1] E. L. Saldin, E.V. Schneidmiller, and M. V. Yurkov, "*The physics of free electron lasers*", Springer Science & Business Media, 2013.

[2] A. Gover, "Laser: Free election lasers," in Encyclopaedia of Modern Optics, R. D. Guenther, D. G. Steel, and L. Bayvel, Eds. New York, NY, USA: Elsevier, 2005. [Online]. Available: http://www.eng.tau. ac.il/research/FEL/Encyclopedia%20of%20Modern%20Optics1.pdf

[3] L. R. Elias, J. Hu, G. Ramian, "The UCSB electrostatic accelerator free electron laser: First operation." *Nuclear Instruments and Methods in Physics Research Section A: Accelerators, Spectrometers, Detectors and Associated Equipment*, vol. 237, no. 1, pp. 203-206, 1985.

[4] A. Amir, L. R. Elias, R. J. Hu, G. Ramian, "Spectral characteristics of the UCSB free-electron laser." *Technical Symposium Southeast*. International Society for Optics and Photonics. pp. 20-22, Sept. 1987.

[5] Verhoeven, A. G. A., W. A. Bongers, V. L. Bratman, M. Caplan, G. G. Denisov, C. A. J. Van Der Geer, P. Manintveld et al. "First microwave generation in the FOM free-electron maser." *Plasma physics and controlled fusion*, vol. 40, no. 8A, p. 139, 1998.

[6] B. C. Lee, S. K. Kim, Y. U. Jeong, S. O. Cho, B. H. Cha, J. Lee, "First lasing of the KAERI millimeter-wave free electron laser." *Nuclear Instruments and Methods in Physics Research Section A: Accelerators, Spectrometers, Detectors and Associated Equipment*, vol. 375, no. 1, pp. 28-31, 1996.

[7] G. R. Neil, "FEL oscillators", *Proceedings of the IEEE*, PAC 2003, vol. 1, pp. 181-185, 2003.

[8] A. W. Cross, A. J. MacLachlan, C. W. Robertson, L. Zhang, K. Ronald, and A. D. R. Phelps. "Highly overmoded MM-wave oscillator experiments." In *2019 12th UK-Europe-China Workshop on Millimeter Waves and Terahertz Technologies (UCMMT)*, pp. 1-2. IEEE, 2019.

[9] N.Y. Peskov, N.S. Ginzburg, I.I. Golubev, S.M. Golubykh, A.K. Kaminsky, A.P. Kozlov, A.M. Malkin, S.N. Sedykh, A.S. Sergeev, A.I. Sidorov, and V.Y. Zaslavsky, "Powerful oversized W-band free-electron maser with advanced Bragg resonator based on coupling of propagating and cutoff waves", *Applied Physics Letters*, *116*(21), p.213505, 2020.

[10] Miginsky, S. V., S. Bae, B. V. Gudkov, T. Yoon, and Y. U. Jeong. "Progress on the Compact THz FEL at KAERI." Bulletin of the Russian Academy of Sciences: Physics 82, no. 12, 1604-1606, 2018.

[11] Yu S. Oparina, N. Yu Peskov, and A. V. Savilov. "Electron rf Oscillator Based on Self-Excitation of a Talbot-Type Supermode in an Oversized Cavity." *Physical Review Applied* 12, no. 4 (2019): 044070.

[12] K. Kawase, M. Nagai, K. Furukawa, M. Fujimoto, R. Kato, Y. Honda, and G.Isoyama, "Extremely high-intensity operation of a THz free-electron laser using an electron beam with a higher bunch charge." Nuclear Instruments and Methods in Physics Research Section A: Accelerators, Spectrometers, Detectors and Associated Equipment 960, 163582, 2020.

[13] P. Sprangle, Cha-Mei Tang, W. M. Manheimer, "Nonlinear theory of free-electron lasers and efficiency enhancement." *Physical Review A*, vol. 21, no. 1, p. 302, Jan. 1980.

[14] N. M. Kroll, P. L. Morton, M. N. Rosenbluth, "Free-Electron Lasers with Variable Parameter Wigglers", *IEEE Journal of Quantum Electronics*, vol. 17, no. 8, Aug. 1981.

[15] Wang, X. J., H. P. Freund, D. Harder, W. H. Miner Jr, J. B. Murphy, H. Qian, Y. Shen, and X. Yang. "Efficiency and spectrum enhancement in a tapered free-electron laser amplifier." *Physical review letters* 103, no. 15, p. 154801, Oct. 2009.

[16] Y. Hidaka et al., "Experimental investigation of superradiance in a tapered free-electron laser amplifier," Proc. 2011 Part. Acc. Conference, New York, USA, THP148, pp. 2396-2398, 2011.

[17] Freund, H. P. "Comparison of free-electron laser amplifiers based on a step-tapered optical klystron and a conventional tapered wiggler." *Physical Review Special Topics-Accelerators and Beams* vol. 16, no. 6, p. 060701, Jun. 2013

[18] E. A. Schneidmiller, M. V. Yurkov. "Optimization of a high efficiency free electron laser amplifier." *Physical Review Special Topics-Accelerators and Beams*, vol. 18, no. 3, p. 030705, March 2015.

[19] A. Curcio, G. Dattoli, E. Di Palma, A. Petralia, "Free electron laser oscillator efficiency." *Optics Communications* 425, 29-37, 2018.

[20] J. Duris, P. Musumeci, N. Sudar, A. Murokh, A. Gover, "Tapering enhanced stimulated superradiant oscillator." *Physical Review Accelerators and Beams*, *21*(8), 080705, 2018.

[21] Eecen, P. J., T. J. Schep, and A. V. Tulupov. "Spectral dynamics of a free-electron maser with a step-tapered undulator." *Physical Review E* 52, no. 5: 5460, 1995

[22] A. Yariv, "Introduction to Optical Optoelectronics", Holt, Rinehart and Winston, Inc., 1971.

[23] V. Kubarev, and Y. U. Jeong, "Comprehensive analytical optimization of the hybrid optical resonator of the KAERI compact terahertz free-electron laser." Nuclear Instruments and Methods in Physics Research Section A: Accelerators, Spectrometers, Detectors and Associated Equipment 930 (2019): 173-179.

[24] H. S. Marks, A. Gover, D. Borodin, A. Damti, M. Kanter, Y. Lasser, M. Einat, Y. Vashdi, Y. Lurie, and A. Friedman, "Radiation Power Out-Coupling Optimization of a Free Electron Laser Oscillator, " *IEEE Transactions on Microwave Theory and Techniques*, vol. 64, no. 3, pp. 1006-1014, Mar. 2016.

[25] Gover, Avi. "Superradiant and stimulated-superradiant emission in prebunched electron-beam radiators. I. Formulation." *Physical Review Special Topics-Accelerators and Beams* 8, no. 3 (2005): 030701.

[26] Gover, A., E. Dyunin, Y. Lurie, Y. Pinhasi, and M. V. Krongauz. "Superradiant and stimulated-superradiant emission in prebunched electron-beam radiators. II. Radiation enhancement schemes." *Physical Review Special Topics-Accelerators and Beams* 8, no. 3: 030702, 2005.

[27] H. S. Marks, Yu Lurie, E. Dyunin, and A. Gover, "Enhancing Electron Beam Radiative Energy Extraction Efficiency in Free-Electron Laser Oscillators Through Beam Energy Ramping," *IEEE Transactions on Microwave Theory and Techniques*, May, 2017.

[28] Xu Y, Jia Q, Li H. “Efficiency enhancement of RF-linac based free electron laser oscillator with electron beam energy ramping.” Nuclear Instruments and Methods in Physics Research Section A: Accelerators, Spectrometers, Detectors and Associated Equipment. Oct 1; 940:448-52, 2019
[29] R. Hellborg, “Electrostatic accelerators”, Springer-Verlag Berlin Heidelberg, 2005.
[30] L.A. Rivlin, V.S. Shul'dyaev, “Multimode waveguides for coherent light”, *Radiophys Quantum Electron* **11,** 318–321, 1968. https://doi.org/10.1007/BF01038737
[31] G. G. Denisov, D. A. Lukovnikov, and M. Yu Shmelyov. "Digest of 18 Int." In *Conf. on IR and MM Waves, Colchester, UK*, vol. 485. 1993.
[32] H.S. Marks, and A. Gover, “Talbot effect mm-wave resonator for an electrostatic accelerator free electron laser.” *IEEE Transactions on Microwave Theory and Techniques*, *66*(1), pp.3-10, 2017.
[33] Y. Pinhasi, M. Cohen, A. Gover, “Three-dimensional codes for simulating electron beam transport and free-electron laser operation including space-charge effects.” *Int. J. Electron.*, vol. 78, no. 3, pp. 581-50, 1995.
[34] A. Abramovich, Y. Pinhasi, A. Yahalom, D. Bar-Lev, S. Efimov, and A. Gover. "Optimization of power output and study of electron beam energy spread in a Free Electron Laser oscillator." Nuclear Instruments and Methods in Physics Research Section A: Accelerators, Spectrometers, Detectors and Associated Equipment 475, no. 1-3, pp. 579-582, 2001.